

# Bulk Mode Piezoresistive Thermal Oscillators: Time Constants and Scaling

Subramanian Sundaram and Dana Weinstein, *Member, IEEE*

**Abstract**—This paper presents design and analysis for engineering the thermal and mechanical time constants of piezoresistive thermal oscillators. The optimal design is obtained by minimizing the threshold current density required to initiate self-sustained oscillations. Optimizing the oscillator geometry is of extreme practical importance given that the threshold current densities ( $\text{GA}/\text{m}^2$ ) are close to the breakdown current densities observed in silicon. The equivalent circuit model of the oscillator is used along with the lumped thermal, mechanical, and piezoresistive parameters to calculate the threshold current density of the oscillator. The optimal ratio of the thermal and mechanical time constants is found to be  $\sqrt{3}$  for bulk-mode oscillators where the in-plane dimensions control the mechanical resonant frequency. The final frequency of oscillations is obtained as a function of the mechanical resonant frequency, quality factor ( $Q$ ), and the ratio of the time constants. Results show that scaling the dimension (or frequency) has a weak sub-linear effect on the oscillator performance. Finally, we compare different bulk modes, based on the calculated threshold dc currents for a 1-GHz oscillator.

## I. INTRODUCTION

MICROELECTROMECHANICAL (MEMS) resonators and oscillators have emerged as front runners for RF front-ends, high frequency filters, and frequency sources for various applications in the past two decades. MEMS oscillators have bridged the gap between high-performance quartz-based frequency references and on-chip electrical oscillators, and over the past decade, have rivalled quartz-based references in all performance metrics such as power dissipation, frequency stability, and accuracy. The prospect of seamless integration with CMOS has provided a significant boost to displace quartz, which has been the go-to option for timing sources for a long time [1], [2].

Until now, MEMS resonators have been used with an active feedback amplifier to construct an oscillator. Best reported frequency-quality factor products ( $fQ$ , the common figure of merit) of these resonators have consistently reached  $10^{13}$  to  $10^{14}$  Hz. However, the design of the feedback amplifier can be a major hurdle at very high frequencies. A MEMS oscillator with an intrinsic feedback mechanism overcomes the need for an electronic amplifier and the parasitics that have to be accounted for, as all the signals involved in the feedback are confined within the device. Designing an all-MEMS oscillator is challeng-

ing and has not been explored much. Steeneken *et al.* [3] demonstrated that a thermally actuated resonator starts to oscillate spontaneously when subjected to large dc bias currents. The piezoresistive-thermal feedback mechanism compensates for the damping, and provides a closed loop unity gain path once the bias current threshold is reached. The flexural resonant modes used in the work restricts these devices to low frequencies. However, the low-frequency devices with low threshold current densities provided a convenient platform to demonstrate 1.26-MHz oscillators and the working mechanism.

The device can be simplified as a narrow actuator and resonator pair. When large currents are forced through the narrow beam, Joule heating causes it to expand, and overshoot. The elongation of the beam causes a drop in the resistance, due to a large negative longitudinal piezoresistance coefficient. This further leads to a reduction in the heat generated, causing it to contract, and have an increase in resistance. This process occurs repeatedly and constitutes the feedback path. The sinusoidally time varying resistance multiplied by a large dc bias current appears as the voltage output across the device.

The mechanism was utilized with a dual plate geometry to increase the oscillation frequencies, up to 161 MHz [4], [5]. Using a similar geometry, two modes have been excited simultaneously, using the bias current to control the strength of the two modes [6]. Recent work [7] demonstrates a low power oscillator ( $70 \mu\text{W}$ ), but at an oscillation frequency of 740 kHz. Given that the threshold current density for reaching sustained oscillations is very high, it is important to focus on optimizing the device geometry to lower the threshold. There is a lack of a methodology for optimizing these devices. The devices demonstrated thus far are similar, where the mechanical stiffness and the effective proof mass have been decoupled. Further, the maximum frequencies attainable is unclear, and there is no systemic understanding on how to expand these limits. Here we focus on addressing these issues, developing insights into optimizing the device geometries, looking at the thermal and mechanical time constants in bulk mode devices, with the goal of exploring designs capable of reaching much higher frequencies.

## II. SILICON PIEZORESISTIVE THERMAL OSCILLATOR

The oscillator described here consists of mechanical, piezoresistive, and thermal components that work in unison to satisfy the Barkhausen criteria. The mechanical and

Manuscript received December 3, 2014; accepted May 5, 2015.

The authors are with the Department of Electrical Engineering and Computer Science, Massachusetts Institute of Technology, Cambridge, MA 02139, USA (e-mail: subras@mit.edu).

DOI <http://dx.doi.org/10.1109/TUFFC.2014.006918>

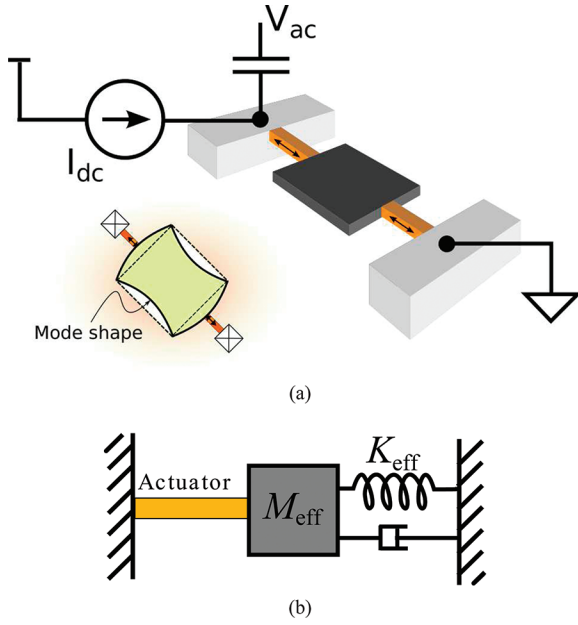


Fig. 1. (a) Schematic of a bulk (Lamé) mode oscillator with two actuators. The dc bias current flows through the actuators and the square proof mass. The inset on the bottom left shows the mode shape. (b) Lumped model of the piezoresistive thermal oscillator showing the thermal actuator, effective mass, stiffness, and damping components. For bulk mode oscillators, the proof mass contributes both the effective mass  $M_{\text{eff}}$  and the stiffness  $K_{\text{eff}}$ .

thermal characteristics can be carefully tuned by varying the geometry, which is envisioned to be designed in the device layer, using a SOI-MEMS process. The structure is freely suspended by removing the underlying buried oxide. The device consists of a narrow beam called the actuator and mechanical components that make up the resonator: the actuator compensates for the energy lost during each cycle, and the resonator is the frequency selective element. Fig. 1(a) shows the proposed bulk mode oscillator (Lamé mode oscillator in this case) and the driving circuit. The oscillator has two supports that are also the actuators (in yellow), and the square proof mass is the frequency selective component. This work provides a new perspective on picking the dimensions of the actuators and their relationship with the critical frequency deciding component (the side of square for the Lamé mode). It is useful to abstract the oscillator to the 1-D mass-spring-dashpot system shown in Fig. 1(b). Once set into oscillations and the self-limiting amplitude is reached, the actuator pumps in exactly the same quantum of energy lost each cycle due to all damping mechanisms lumped as the dashpot. The effective mass  $M_{\text{eff}}$  and the spring stiffness  $K_{\text{eff}}$  are both decided by the resonator geometry in bulk modes.

Fig. 2 shows the feedback loop and the various transformations involved: displacement,  $x$ , to change in resistance,  $r_{\text{ac}}$ , via the piezoresistance coefficient  $\rightarrow$  change in resistance to change in heat generated via Joule heating  $\rightarrow$  change in temperature  $T$  leading to a change in the displacement via thermal expansion. The total phase shift through the closed loop feedback system is  $n(2\pi)$ ,  $n \in \mathbb{N}$ .

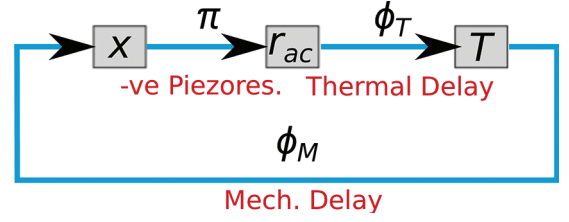


Fig. 2. Feedback loop showing the displacement  $x$ , resistance  $r_{\text{ac}}$ , and the temperature  $T$ .  $\pi$  accounts for the sign inversion in the transformation between  $x$  and  $r_{\text{ac}}$ .  $\phi_T$  and  $\phi_M$  are the thermal and mechanical phase shifts.

In Fig. 2,  $\pi$  indicates the  $180^\circ$  phase shift from displacement to change in the resistance, in the feedback loop. This stems from the fact that the longitudinal piezoresistive coefficient is negative in  $n$ -type silicon along [100].  $\phi_T$  and  $\phi_M$  denote the phase shift from the thermal and mechanical components, and  $\phi_T + \phi_M = (2n + 1)\pi$ ,  $n \in \mathbb{N}$ . The actuators are oriented along the direction with the largest (most negative) longitudinal piezoresistive coefficient,  $\pi_1 = -102.2 \times 10^{-11}/\text{Pa}$  (along the [100] direction in  $n$ -type single crystal silicon) [8], [9]. In general, the piezoresistance observed in silicon is nonlinear but under conditions of small applied stresses, it can be modeled linearly using the piezoresistive coefficient. Typically, for donor concentrations  $N_D > 10^{19}/\text{cm}^2$ , the piezoresistive effect becomes less effective; however, there is nearly a 50% boost as the temperature is lowered from room temperature to 200K [9]. The negative sign of the piezoresistive coefficient (phase shift of  $\pi$ ) plays a crucial role in the working of the oscillator.

The actuator is a narrow beam that dominates the overall resistance in the current pathway. As current flows through the narrow channel, the temperature responds to changes in the heat generated, as a result of Joule heating, with a first-order linear time invariant response. Microthermal actuators generate a large force and displacement, and operate at lower voltages compared with their electrostatic counterparts. The time required for actuation is of the order of the thermal time constant,  $\tau_T$ , which is also a factor that decides the thermal phase shift  $\phi_T$ , based on the operational frequency  $\omega$ . We have considered straight narrow beam actuators oriented along the equivalent  $\langle 100 \rangle$  directions, with similar material properties. In this design, longitudinal displacement of the actuator is used to actuate the device effectively. Other actuator geometries can be used if their displacements can coherently transfer energy into the oscillator.

### III. MODEL: THRESHOLD CURRENT DENSITY WITH BULK MODE APPROXIMATION

The oscillation frequency and the threshold current required to set the oscillator into spontaneous oscillations are key parameters that are needed to evaluate the performance of the oscillator. Current densities required for

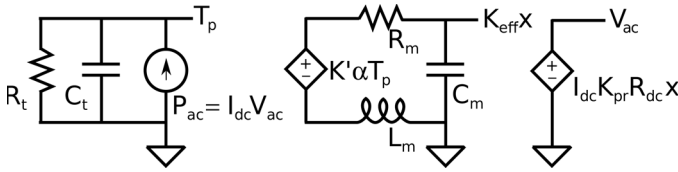


Fig. 3. Equivalent circuit diagram showing the thermal, mechanical, and piezoresistive sections.

sustaining oscillations, reported in earlier works (e.g., 2.83 GA/m<sup>2</sup> in [3]) and the range of measured breakdown current densities in silicon are extremely close. So designing to minimize the current threshold is crucial. Thermal, mechanical, and piezoresistive effects are modeled into the equivalent circuit diagram (modified version of circuit in [10], with  $K'$  different from  $K_{\text{eff}}$ ), shown in Fig. 3, to develop analytical models for the threshold current density and understand the factors involved. Table I lists the circuit variables and their descriptions. The thermal R-C loop (left in Fig. 3) models the thermal actuator, which is a first-order system with a lumped thermal resistance,  $R_t$ , and thermal capacitance,  $C_t$ . The thermal section models the temperature as a function of the Joule heating power input ( $P_{\text{ac}}$ ). The mechanical circuit in the middle models the displacement in response to the thermal expansion force  $K'\alpha T_p$ , where  $K'$  is the equivalent stiffness of the thermal actuator (defined in the Appendix). The transfer function between the displacement and the generated small signal voltage is shown on the right in Fig. 3.

For a narrow beam actuator with a cross section area  $A$ , the lumped thermal parameters are obtained as

$$R_t = \frac{L}{8k_{\text{th}}A}, \quad (1a)$$

$$C_t = \frac{2}{3}C_p\rho_MAL, \quad (1b)$$

where  $L$  is the length of the actuator,  $k_{\text{th}}$  is the thermal conductivity,  $C_p$  is the specific heat capacity, and  $\rho_M$  is the density. These parameters are obtained by lumping the temperature at the center of the actuator beam ( $T_p$ ) with thermal grounds at the two ends; the full derivation is in the Appendix. The mechanical lumped parameters  $R_m$ ,  $C_m$ , and  $L_m$  are dependent on the modes and on the damping mechanisms. The effective masses and spring stiffnesses are well known for common modes; additional description is in Section V. The standard equation of motion is  $\ddot{x} + (\omega_0/Q)\dot{x} + \omega_0^2x = F/M_{\text{eff}}$ , where  $\omega_0$  is the mechanical resonant frequency. The forcing function  $F$  is given as

$$F = K'\alpha I_{\text{dc}}^2 K_{\text{pr}} R_{\text{dc}} \left( \frac{R_t}{1 + j\omega R_t C_t} \right) x, \quad (2)$$

with the proportionality constant  $K_{\text{pr}} = E\pi_1/L$ , where  $E$  is the Young's modulus. The variation in the resistance  $r_{\text{ac}}$  is written as  $r_{\text{ac}} = K_{\text{pr}}xR_{\text{dc}}$ , where  $R_{\text{dc}}$  is the total resistance in the current path. If the effective number of actuators

TABLE I. DESCRIPTION OF THE CIRCUIT PARAMETERS.

Variable	Description
$R_t$	Equivalent thermal resistance (K/W)
$C_t$	Equivalent thermal capacitance (J/K)
$P_{\text{ac}}$	Joule heating power (W)
$T_p$	Spatial-peak ac temperature (K)
$I_{\text{dc}}$	Constant bias current in the oscillator (A)
$V_{\text{ac}}$	ac voltage (oscillator output) (V)
$K'$	Equivalent stiffness of the thermal actuator (N/m)
$\alpha$	Thermal expansion coefficient (length accounted) (m/K)
$R_m$	Lumped equivalent mechanical resistance (kg-rad/s)
$C_m$	Lumped equivalent mechanical capacitance (m/N)
$L_m$	Lumped equivalent mechanical inductance (Kg)
$x$	Displacement of the resonator (m)
$r_{\text{ac}}$	Resistance variation (ac) due to the piezoresistive effect ( $\Omega$ )
$R_{\text{dc}}$	Resistance of the structure ( $\Omega$ )

in series in the current path is  $n_{\text{el}}$ , then  $R_{\text{dc}} = n_{\text{el}}L/(\sigma_e A)$ , where  $\sigma_e$  is the electrical conductivity.

Assuming a solution of the form  $x = x_0 e^{-j\omega t}$  for the standard equation of motion, and equating the imaginary components to 0 as damping is effectively eliminated (condition for sustained oscillations), the dc threshold current is obtained as

$$I_{\text{th}} = \sqrt{M_{\text{eff}} \frac{\omega_0}{Q} \frac{1 + (\omega R_t C_t)^2}{K'\alpha K_{\text{pr}} R_{\text{dc}} C_t R_t^2}}, \quad (3)$$

where  $\omega$  is the final frequency of oscillation, which is set by the phase shift condition described earlier. This requires that

$$\begin{aligned} \phi_T + \phi_M &= \tan^{-1}(-\omega\tau_T) + \tan^{-1}\left(-\frac{\omega}{Q} \frac{\omega_0}{\omega_0^2 - \omega^2}\right) \\ &= (2n - 1)\pi, \quad n \in \mathbb{Z}. \end{aligned} \quad (4)$$

This need to meet the phase shift condition of the Barkhausen criteria highlights an important tradeoff in these oscillators. It is well known that the phase shift between the input force and the output displacement for a second-order simple harmonic oscillator is  $\sim -\pi/2$  near the resonant frequency, where the amplitude of oscillations is maximum. However, for the thermal delay to account for the other  $-\pi/2$ , the oscillation frequency would have to be much higher than the pole frequency in the first-order thermal system. This would result in a smaller temperature, which reduces the magnitude of the thermal force in the feedback loop. On the other hand, if the oscillation frequency was far away from natural frequency of the mechanical system, the displacement amplitude rolls off sharply and leads to smaller stresses leading to smaller piezoresistive feedback in the system. The final oscillation frequency that the system falls into is picked by the system naturally such that the phase shift criterion is met, and is higher than the mechanical frequency yet not too far away from it. The above condition implies that the final frequency of oscillation is obtained as

$$\omega = \omega_0 \sqrt{1 + \left(\frac{\tau_M}{\tau_T}\right) \frac{1}{Q}}, \quad (5)$$

where  $\tau_M$  is the mechanical time constant and is equal to  $1/\omega_0$ . Eq. (5) shows that the final settling frequency of the oscillator depends on the ratio of the thermal and mechanical time constants and the mechanical quality factor of the resonator. Under normal conditions with  $Q \gg 1$ , the oscillation frequency is less sensitive to the ratio of the time constants and close to the mechanical resonant frequency. Substituting this in the threshold current equation, we get

$$I_{\text{th}} = \sqrt{\frac{M_{\text{eff}}}{Q\tau_M} \left\{ 1 + \frac{\tau_T}{\tau_M Q} + \left(\frac{\tau_T}{\tau_M}\right)^2 \right\} \frac{1}{K'\alpha K_{\text{pr}} R_{\text{dc}} R_{\text{t}} \tau_T}}. \quad (6)$$

This gives the threshold current density for an oscillator, where the time constants  $\tau_M$  and  $\tau_T$  are set by the geometry.

#### IV. TIME CONSTANTS AND SCALING

From (5) and (6), it is clear that the time constants and their ratio play an important role in all metrics of the oscillator. For bulk modes, the mechanical time constant (the inverse of the resonant frequency  $\omega_0$ ) can be generalized as

$$\tau_M = \frac{1}{\omega_0} = \frac{D_M}{\beta_{\text{mode}}} \sqrt{\frac{\rho_M}{E}}, \quad (7)$$

where  $\beta_{\text{mode}}$  is a modeshape dependent constant and  $D_M$  is the dominant in-plane dimension that sets the oscillation frequency. This equation shows that mechanical time constant is directly proportional to the critical dimension of the mode and inversely proportional to the acoustic velocity.

The effective mass is proportional to the physical mass of the device, where the proportionality constant, say  $x_{\text{ME}}$ , can be calculated based on the mode shape. In particular, for bulk mode devices, the effective mass can be defined simply as

$$M_{\text{eff}} = x_{\text{ME}} \rho_M D_M^2 T_M, \quad (8)$$

where  $T_M$  is the thickness, in this case, of the SOI device layer. Section V includes a detailed explanation on  $x_{\text{ME}}$ ,  $D_M$ , and  $\beta_{\text{mode}}$  for a few commonly used bulk modes.

The thermal time constant is obtained by combining the thermal resistance and capacitance in (1), and is given by

$$\tau_T = \frac{C_p \rho_M L^2}{12k_{\text{th}}}. \quad (9)$$

It is seen that the thermal time constant is independent of the area of cross section of the actuator, and is purely dependent on the length.

Based on (7) and (9), the ratio of the time constants is given by

$$\frac{\tau_T}{\tau_M} = \frac{C_p \beta_{\text{mode}} \sqrt{E \rho_M} L^2}{12k_{\text{th}} D_M}. \quad (10)$$

Using this, the threshold current density  $J_{\text{th}}$  is obtained as

$$J_{\text{th}}^2 = \chi \frac{T_M}{A\sqrt{D_M}} \left\{ \left(\frac{\tau_M}{\tau_T}\right)^{1.5} + \frac{1}{Q} \left(\frac{\tau_M}{\tau_T}\right)^{0.5} + \left(\frac{\tau_M}{\tau_T}\right)^{-0.5} \right\}, \quad (11a)$$

$$\chi = 2\sqrt{3} \frac{x_{\text{ME}} \sigma_e \rho_M^{0.25} k_{\text{th}}^{0.5} C_p^{0.5} \beta_{\text{mode}}^{2.5}}{QE^{0.75} \alpha_t \pi n_{\text{el}}}, \quad (11b)$$

where  $\chi$  is a constant defined as above. For a desired frequency (fixing  $D_M$ ), the optimal ratio of the time constants can be computed by minimizing (11a), since  $T_M$  and  $A$  do not influence the ratio of the time constants. Using this approach, the optimal ratio of the time constants is obtained as

$$\left(\frac{\tau_M}{\tau_T}\right)_{\text{opt}} = \sqrt{\left(\frac{1}{6Q}\right)^2 + \frac{1}{3}} - \frac{1}{6Q} \approx \frac{1}{\sqrt{3}} \quad (12)$$

in the typical range of values for  $Q$  ( $Q \gg 1$ ). Therefore, the optimal length of actuators in terms of  $D_M$  is

$$L_{\text{opt}} = \sqrt{\frac{12\sqrt{3}k_{\text{th}}}{C_p \beta_{\text{mode}} \sqrt{E \rho_M}}} D_M. \quad (13)$$

Substituting these results in (11a), we get the minimum threshold current density to be

$$J_{\text{th}}^2 |_{\text{min}} \approx 1.75\chi \frac{T_M}{A\sqrt{D_M}}. \quad (14)$$

Understanding how the threshold current density scales with the frequency is of significant interest. From (14) it is seen that the threshold current density reduces with increase in the characteristic mechanical dimension  $D_M$ , with the following relationship:

$$J_{\text{th}} \propto \frac{1}{D_M^{0.25}} \propto \omega_0^{0.25}. \quad (15)$$

As we operate at higher frequencies, and the dimensions shrink, the minimum threshold current density increases, though sublinearly.

Device optimization performed here is primarily focused on minimizing the threshold current density, to explore the gamut of practical designs. It is important to note that the analytical framework developed here can be subsequently used to optimize device design based on other key metrics such as peak device temperature, power consumption and noise.

TABLE II.  $x_{\text{ME}}$  AND  $\beta_{\text{MODE}}$  FOR COMMON MODES.

Mode	$D_{\text{M}}$	$x_{\text{ME}}$	$\beta_{\text{mode}}$
Lamé	$L_1$	0.5	$\pi/\sqrt{(1+\nu)}$
Square extensional	$L_{\text{se}}$	1	$\pi$
Radial extensional (disk)	$R_{\text{d}}$	Eq. (22)	$\sim 0.684\pi$
Wineglass (disk)	$R_{\text{d}}$	Eq. (24)	$\sim 0.544\pi$
Extensional wineglass (ring)	$R_{\text{o}} - R_{\text{i}}$	Eq. (26)	0.5

## V. LUMPED MECHANICAL PARAMETERS OF COMMON BULK MODES

Various bulk mode resonators have been used frequently (seen in Fig. 4), with improving  $fQ$  products. In particular, the Lamé mode, square extensional mode, radial and wineglass disk modes, and extensional-wineglass ring mode are considered here. These modes offer a possibility to reduce the damping losses by careful anchor design. Analytical and numerical approaches to calculate the resonant frequency and the lumped parameters of these modes have been derived in the past, and here we relate these parameters to the specific derived parameters used in our work. In particular, we talk about  $x_{\text{ME}}$  (effective mass constant),  $D_{\text{M}}$  (critical dimension), and  $\beta_{\text{mode}}$  (mode-dependent constant) for each of these modes, listed in Table II.

### A. Lamé Mode

The Lamé mode is an isochoric mode that can be excited in rectangular resonators. The first-order Lamé mode has 4 quasi-nodal points (zero displacement), and the points of maximum displacement are at the centers of the sides. In general resonator design, supports are placed at the quasi-nodal points to reduce loss of acoustic energy through the anchors. However, here the supports are placed at the points of maximum displacement to actuate the mode effectively. The lumped mass and stiffness of the Lamé mode are calculated as

$$M_{\text{eff}} = \frac{1}{2} \rho_{\text{M}} T_{\text{M}} L_1^2, \quad (16a)$$

$$k_{\text{eff}} = \frac{1}{2(1+\nu)} \pi^2 E T_{\text{M}}, \quad (16b)$$

where  $L_1$  is the side of the square, and  $\nu$  is the Poisson's ratio. Comparing this with (8) gives  $x_{\text{ME}} = 0.5$  with the length  $L_1$  as the dominant in-plane dimension. The resonant frequency of the Lamé mode is [11]

$$\omega_0 = \frac{\pi}{L_1} \sqrt{\frac{E}{(1+\nu)\rho_{\text{M}}}}. \quad (17)$$

This gives  $\beta_{\text{mode}} = \pi/\sqrt{(1+\nu)}$  for the Lamé mode, from (7).

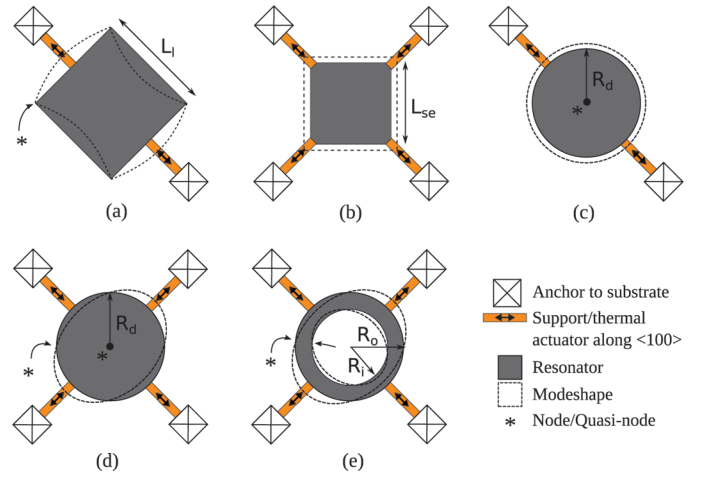


Fig. 4. Common bulk-mode resonator schematics. (a) Lamé mode, (b) square extensional mode, (c) radial disk mode, (d) disk wineglass mode, and (e) ring extensional wineglass mode. Dashed lines show the mode shape. \* indicates the nodes and quasi-nodes. The proof masses and supports are freely suspended, and the anchors are fixed rigidly to the substrate.

### B. Square Extensional Mode

The modeshape of the square extensional mode is approximated as a uniformly expanding square, as seen in Fig. 4(b). In general, the modeshape does not allow for a convenient planar nodal support. Here the actuators are placed at the 4 corners that actuate the structure uniformly. The equivalent mechanical parameters, lumped at the corner of the square extensional mode, is given by [12]

$$M_{\text{eff}} = \rho_{\text{M}} T_{\text{M}} L_{\text{se}}^2, \quad (18a)$$

$$k_{\text{eff}} = \pi^2 E T_{\text{M}}, \quad (18b)$$

where  $L_{\text{se}}$  is the size of the square. This implies  $x_{\text{ME}} = 1$ , from (8), with  $L_{\text{se}}$  as the critical dimension. Based on this, the resonant frequency is obtained as

$$\omega_0 = \frac{\pi}{L_{\text{se}}} \sqrt{\frac{E}{\rho_{\text{M}}}}. \quad (19)$$

Eq. (7) gives  $\beta_{\text{mode}} = \pi$  for the square extensional mode.

### C. Radial Disk Mode

The first-order radial disk mode consists of an expanding and contracting disk (radially). Radial disk modes have a nodal point at the center and can be supported with a stem at the center. Radial actuators are used here to support and actuate the device. The set of radial modes was analyzed by Onoe [13]. The resonant frequency of the first radial disk mode for a disk with radius  $R_{\text{d}}$  is obtained by finding a numerical solution to the equation [14]

$$\frac{J_0\left(\frac{\zeta}{\xi}\right)}{J_1\left(\frac{\zeta}{\xi}\right)} = 1 - \nu, \quad (20a)$$

$$\zeta = \omega_0 R_d \sqrt{\frac{2\rho_M(1+\nu)}{E}}, \quad (20b)$$

$$\xi = \sqrt{\frac{2}{1-\nu}}, \quad (20c)$$

where  $J_i(n)$  is the Bessel function of the first kind, of order  $i$ . Exact solutions of (20) can be approximated with a more intuitive form [15]:

$$\omega_0 = \frac{(0.342)2\pi}{R_d} \sqrt{\frac{E}{\rho}}, \quad (21)$$

$\beta_{\text{mode}} = 0.684\pi$  for the radial disk mode with the radius as the critical dimension  $D_M$ . The effective mass coefficient,  $x_{\text{ME}}$ , seen at the perimeter of the disk is given by

$$x_{\text{ME}} = \frac{M_{\text{eff}}}{\rho_M T_M R_d^2} = \frac{2\pi}{R_d^2 J_1(hR_d)^2} \int_0^{R_d} r J_1(hr)^2 dr. \quad (22)$$

Numerically,  $x_{\text{ME}} \approx 0.79\pi$  for the first-order radial disk mode using  $D_M = R_d$ , as defined in (8).

#### D. Wineglass Disk Mode

The wineglass mode, shown in Fig. 4(d), has 4 quasi-nodes along the perimeter and one node at the center of the disk of radius  $R_d$ . The exact solution to the resonant frequency of this mode is obtained numerically (see [13]). The resonant frequency can be approximately written as [15]

$$\omega_0 = \frac{(0.272)2\pi}{R_d} \sqrt{\frac{E}{\rho_M}}. \quad (23)$$

This implies  $\beta_{\text{mode}} = 0.544\pi$  for the first-order mode. The effective mass is given by

$$x_{\text{ME}} = \frac{1}{R_d^2 U^2 |_{r=R_d, \theta=0}} \int_0^{R_d} \int_0^{2\pi} (U^2 + V^2) r d\theta \cdot dr, \quad (24)$$

where  $U$  and  $V$  are the radial and tangential displacement at the point in the structure. Expressions for  $U$  and  $V$  are described in [13].  $x_{\text{ME}}$  can be obtained numerically from the above equation.

#### E. Extensional Wineglass Ring Mode

Fig. 4(e) shows the extensional wineglass ring mode, with 4 quasi-nodal points at the outer and inner surfaces. The mode also consists of a nodal circle positioned between  $R_o$  and  $R_i$ . The modeshape consists of alternate quarters expanding and contracting radially. The approximate resonant frequency of the mode is given by [16]

TABLE III. VALUES OF CONSTANTS USED IN CALCULATIONS.

Parameter	Value
Density, $\rho_M$	2330 kg/m <sup>3</sup>
Specific heat capacity, $C_p$	702 J/kg – K
Electrical conductivity, $\sigma$	10 <sup>4</sup> S/m
Thermal conductivity, $k_{\text{th}}$	113 W/m – K
Young's modulus, $E$	180 GPa
Poisson's ratio, $\nu$	0.22
Thermal expansion coefficient, $\alpha_{\text{Si}}$	$2.6 \times 10^{-6}$ K <sup>-1</sup>
Longitudinal piezoresistive coefficient, $\pi_1$	$-102 \times 10^{-11}$ Pa <sup>-1</sup>
Quality factor, $Q$	10 <sup>4</sup>
Device layer thickness, $T_M$	1.5 $\mu\text{m}$

$$\omega_0 = \frac{1}{2(R_o - R_i)} \sqrt{\frac{E}{\rho_M}}. \quad (25)$$

With the radial thickness  $R_o - R_i$  as the critical dimension,  $\beta_{\text{mode}} = 0.5$ . The effective mass is obtained similar to the wineglass disk mode as

$$x_{\text{ME}} = \frac{1}{(R_o - R_i)^2 U^2 |_{r=R_o, \theta=0}} \int_{R_i}^{R_o} \int_0^{2\pi} (U^2 + V^2) r d\theta \cdot dr, \quad (26)$$

where the radial and tangential displacements  $U$  and  $V$  are described in [16], using which  $x_{\text{ME}}$  is numerically estimated.

## VI. RESULTS

Now we proceed to calculate the current at the threshold of oscillations, to estimate feasibility of these devices. Based on the models developed in previous sections, we present a 2-D map of the oscillation threshold density as a function of geometric parameters, to serve as a design guide. Finally, we compare 1-GHz oscillators based on different mode shapes.

The numerical values of the various properties of silicon used in the calculations here are listed in Table III. The quality factor,  $Q$ , of the resonant mode is assumed to be 10<sup>4</sup>, for our calculations. In reality it depends largely on the support design and fabrication process. The highest experimentally reported  $f \cdot Q$  products are  $\sim 10^{14}$ ; hence, the quality factor assumption is invalid at frequencies above  $\sim 10$  GHz.

Let us consider a Lamé mode device [shown in Fig. 4(a)] with a 5- $\mu\text{m}$  side, defined in the device layer of an SOI wafer, with properties defined in Table III. The oscillation frequency of the first Lamé mode is 795.75 MHz (mechanical time constant: 0.2 ns). When the device is actuated by two supports of length 2  $\mu\text{m}$ , and width 1  $\mu\text{m}$  each, the threshold current is obtained as 12.49 mA (current density: 8.32 GA/m<sup>2</sup>). For this design, the ratio of the thermal time constant to the mechanical time constant is 24.12 (thermal time constant: 4.82 ns), far from the optimal ratio. Tuning the length of the support to be

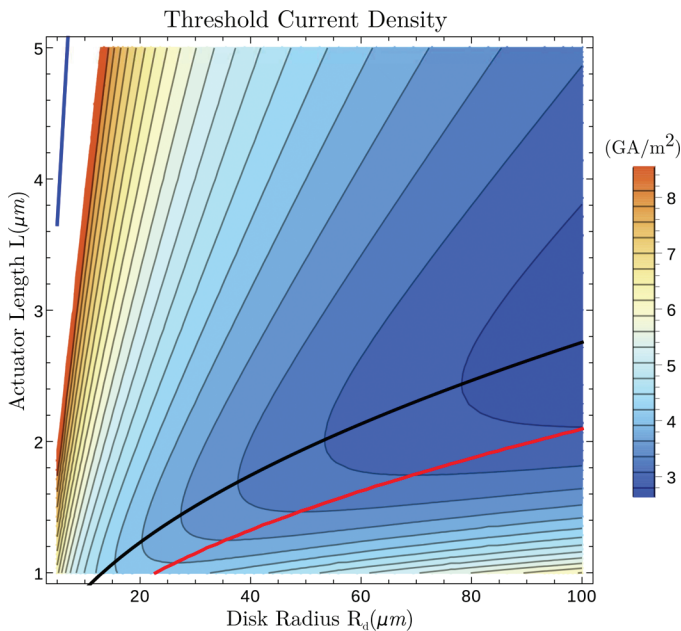


Fig. 5. Contour plot of the threshold current density of a radial disk mode oscillator as a function of the disk radius and the length of the actuator. The thick red, black, and blue curves (top left) map  $\tau_M/\tau_T = 1$ ,  $\tau_M/\tau_T = 1/\sqrt{3}$ , and quarter wavelength actuator conditions. The black curve shows the optimal design given a design frequency. The color bar shows the scale in  $\text{GA}/\text{m}^2$ .

$0.536 \mu\text{m}$ , to match the optimal time constant ratio (thermal time constant for optimal design:  $0.35 \text{ ns}$ ), the threshold current density is  $4.97 \text{ GA}/\text{m}^2$ , a significant improvement over the previous design. It is important to note that this result is obtained assuming a constant quality factor for both designs. In epitaxially grown, suspended silicon nanowires, Wurz *et al.* [17] observed breakdown current densities of approximately  $4 \text{ GA}/\text{m}^2$ . The electrical breakdown in silicon, is driven by the temperature rise in the nanowire, which is a function of the geometry and the material properties. Given that the measured breakdown current densities in silicon are similar to the threshold current densities in these designs, optimizing geometries may very well be the critical link in realizing high frequency self-sustaining oscillators, and exploring the boundaries of the space of working oscillators.

To visualize the device performance in the available parameter space, 2-D contour plots are used. Fig. 5 shows the calculated threshold current density plot for a radial disk mode with 4 supports as a function of the disk radius and the actuator length. The black and red curves show the design with  $\tau_M/\tau_T = 1/\sqrt{3}$ , the optimal design, and the set of devices with  $\tau_M/\tau_T = 1$ . The quality factor, which is assumed to be a constant, normally depends on the actuator length, so the quarter wavelength actuator design is shown for comparison (blue curve, top left). The quarter wavelength actuator is an extremely inefficient design choice if the gains in the quality factor are insignificant.

For a 1-GHz oscillator, the optimal actuator length based on the time constant ratio is  $0.48 \mu\text{m}$ . Table IV

TABLE IV. OPTIMAL DEVICE DIMENSIONS AND THRESHOLD CURRENT DENSITIES FOR 1-GHz OSCILLATORS.

Mode (no. of actuators)	$D_M$ ( $\mu\text{m}$ )	$J_{\text{th,min}}$ ( $\text{GA}/\text{m}^2$ )
Lamé, 2	$L_1 : 3.97$	5.27
Square extensional, 4	$L_{\text{se}} : 4.85$	6.42
Radial extensional (disk), 4	$R_d : 2.86$	6.03
Wineglass (disk), 2	$R_d : 2.09$	5.05
Extensional wineglass (ring), 4	$R_o - R_i : 4.42$	12.8

lists the dimensions and the threshold current densities calculated for 1-GHz oscillators built with different resonant modes. The actuator width is assumed to be  $1 \mu\text{m}$  in these designs. The extensional wineglass mode (with  $R_o = 10 \mu\text{m}$ ) is the least favorable mode, requiring large currents. The Lamé mode and the disk wineglass mode with 2 actuators require the least currents for the desired oscillation frequency. These modes with small dimensions are also susceptible to fabrication mismatches and challenges.

When devices are subjected to large bias currents, required for self-sustaining oscillations, secondary effects such as thermomechanical buckling can lead to undesirable mechanical biases both in plane and out of plane. Such instabilities can force the oscillator into flexural modes and other lower frequency modes. Hence, avoiding acute aspect ratios in the actuator, and evaluating the device stiffness in multiple directions, is an essential part of the practical design process. For these oscillators, the oscillation mode is self selected based on the mode with the highest quality factor requiring the least threshold current density. It is important to be aware and design additional structures that suppress spurious modes, and preferably enhance the quality factor of the desired mode. Although the required threshold current densities are generally high, these devices are promising candidates as high-frequency oscillators.

## VII. CONCLUSION

The relationship between the time constants is established as a crucial factor in optimizing the design of bulk mode piezoresistive thermal oscillators for reduced threshold current densities. The optimal ratio of the thermal and mechanical times constants is obtained as  $\sqrt{3}$ . The large threshold current densities, in the same order as experimentally observed breakdown current densities in silicon, necessitate the need for optimization to realize high frequency devices, and explore the limits of the mechanism. Comparing different bulk modes for use in this oscillator, the Lamé mode and the wineglass (disk) mode are favorable choices, whereas the extensional wineglass (ring) mode suffers from very large oscillation current thresholds. We show that the current threshold required for the onset of oscillations scales weakly with oscillator frequency.

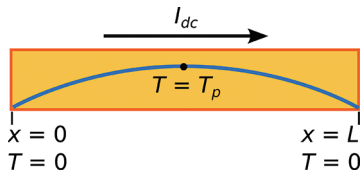


Fig. 6. Actuator beam with the resulting temperature profile due to Joule heating. Assumptions: the ends of the actuator act as thermal sinks, and current generation causes uniform heat generation.

#### APPENDIX THERMAL DOMAIN LUMPED PARAMETERS

In the oscillator design, the actuators are the (functional) thermal parts, which are rapidly heated and cooled at the frequency of oscillation. The thermal loop, seen in the equivalent circuit diagram in Fig. 3 (left block), models the temperature of the narrow-beam actuator as a function of the Joule heating power. The actuator is modeled as a beam of length  $L$  and area of cross section  $A$ , as shown in Fig. 6. The mechanical structures and the anchor to which actuators are attached have significantly larger heat capacities and are considered to be small signal thermal grounds. Assuming that current flows uniformly through the cross section of the beam, and that conduction is the dominant mode of heat transfer, the temperature profile peaks ( $T = T_p$ ) at the center of the beam,  $x = L/2$ .

To find the lumped parameters, we start with the equation for steady-state heat transfer considering heat conduction with uniform heat generation, which is given by [18]

$$\frac{d^2T}{dx^2} = -\frac{J^2\rho_e}{k_{th}}, \quad (27)$$

where  $J$  is the current density,  $\rho_e$  is the electrical resistivity, and  $k_{th}$  is thermal conductivity. Using the boundary conditions  $T = 0$  at  $x = 0$  and  $x = L$ , the temperature profile is obtained as

$$T = \frac{4T_p}{L^2}x(L-x), \quad (28)$$

where  $T_p$  is the spatial temperature peak at the center of the beam, given by  $T_p = J^2\rho_e L^2/(8k_{th})$ . The assumption  $T = 0$  at the ends of the beam is poor for evaluating steady-state temperatures; both the anchor and resonator typically have a nonzero dc temperature. However, the anchor and the resonator make good small signal thermal sinks at the oscillation frequency, given the large disparity in the thermal masses in comparison with the actuator beam. The lumped parameters extracted here are used at the oscillation frequency, where assuming ideal thermal sinks at the two ends of the beam is a valid approximation. All the parameters for the lumped parameter model are obtained by lumping the spatial distribution of properties to the value seen at one point, here, to the longitudinal spatial center of the beam at  $x = L/2$ . The thermal capacitance,

$C_t$ , is found from the total energy stored in the beam, and the temperature of the lumped element,  $T_p$ , as

$$C_t = \frac{Q}{T_p} = \frac{C_p\rho_m A}{T_p} \int_0^L T dx. \quad (29)$$

The effective thermal resistance is calculated, using Ohm's law in the equivalent circuit model in the thermal domain, as

$$R_t = \frac{T_p}{I^2 R_e}, \quad (30)$$

where  $R_e$  is the electrical resistance of the lumped element and  $I^2 R_e$  is the power due to Joule heating. Finally, the effective restoring thermal stiffness of the lumped element,  $K'$ , is calculated by equating the thermal expansion forces,

$$K'\alpha T_p L = \int_0^L K_m \alpha T dx, \quad (31)$$

where  $\alpha$  is the linear thermal expansion coefficient [ $K^{-1}$ ], and  $K_m$  is the mechanical longitudinal stiffness of the actuator. Solving this equation gives  $K' = (2/3)K_m$ , which accounts for lumping the thermal system at the longitudinal center of the beam (while calculating the thermal expansion force at the end of actuator that is free to move, assuming one end is anchored).

#### REFERENCES

- [1] C. T.-C. Nguyen, "MEMS technology for timing and frequency control," *IEEE Trans. Ultrason. Ferroelectr. Freq. Control*, vol. 54, no. 2, pp. 251–270, 2007.
- [2] J. T. M. van Beek and R. Puers, "A review of MEMS oscillators for frequency reference and timing applications," *J. Micromech. Microeng.*, vol. 22, no. 1, art. no. 013001, 2012.
- [3] P. G. Steeneken, K. Le Phan, M. J. Goossens, G. E. J. Koops, G. J. A. M. Brom, C. van der Avoort, and J. T. M. Van Beek, "Piezoresistive heat engine and refrigerator," *Nat. Phys.*, vol. 7, no. 4, pp. 354–359, 2011.
- [4] A. Rahafruz and S. Pourkamali, "Fully micromechanical piezothermal oscillators," in *2010 IEEE Int. Electron Devices Meeting*, pp. 7.2.1–7.2.4.
- [5] H. J. Hall, D. E. Walker, L. Wang, R. C. Fitch, J. S. Bunch, S. Pourkamali, and V. M. Bright, "Mode selection behavior of VHF thermal-piezoresistive self-sustained oscillators," in *17th Int. Conf. on Transducers and Eurosensors XXVII*, 2013, pp. 1392–1395.
- [6] A. Rahafruz and S. H. Pourkamali, "High frequency dual-mode thermal-piezoresistive oscillators," in *2011 Joint Conf. of the IEEE Int. Frequency Control and the European Frequency and Time Forum*, pp. 1–4.
- [7] K.-H. Li, C.-C. Chen, M.-H. Li, and S.-S. Li, "A self-sustained nanomechanical thermal-piezoresistive oscillator with ultra-low power consumption," in *2014 IEEE Int. Electron Devices Meeting*, pp. 1–4.
- [8] S. C. Smith, "Piezoresistance effect in germanium and silicon," *Phys. Rev.*, vol. 94, no. 1, p. 42, 1954.
- [9] Y. Kanda, "A graphical representation of the piezoresistance coefficients in silicon," *IEEE Trans. Electron. Dev.*, vol. 29, no. 1, pp. 64–70, 1982.
- [10] K. L. Phan, P. G. Steeneken, M. J. Goossens, G. E. J. Koops, G. J. A. M. Verheijden, and J. T. M. van Beek, "Spontaneous mechanical oscillation of a DC driven single crystal," arXiv preprint arXiv:0904.3748, 2009.

- [11] S. A. Bhave, D. Gao, R. Maboudian, and R. T. Howe, "Fully-differential poly-SiC Lamé mode resonator and checkerboard filter," *18th IEEE Int. Conf. on Micro Electro Mechanical Systems*, 2005, pp. 223–226.
- [12] V. Kaajakari, T. Mattila, A. Oja, J. Kiihamaki, and H. Seppa, "Square-extensional mode single-crystal silicon micromechanical resonator for low-phase-noise oscillator applications," *IEEE Electron. Device Lett.*, vol. 25, no. 4, pp. 173–175, 2004.
- [13] M. Onoe, "Contour vibrations of isotropic circular plates," *J. Acoust. Soc. Am.*, vol. 28, no. 6, pp. 1158–1162, 1956.
- [14] J. R. Clark, W.-T. Hsu, M. A. Abdelmoneum, and C. T.-C. Nguyen, "High-Q UHF micromechanical radial-contour mode disk resonators," *J. Microelectromechanical Systems*, vol. 14, no. 6, pp. 1298–1310, 2005.
- [15] A. R. Johnson, *Mechanical Filters in Electronics*. New York, NY, USA: John Wiley & Sons, 1983.
- [16] Y. Xie, S.-S. Li, Y.-W. Lin, Z. Ren, and C. T.-C. Nguyen, "1.52-GHz micromechanical extensional wine-glass mode ring resonators," *IEEE Trans. Ultrason. Ferroelectr. Freq. Control*, vol. 55, no. 4, pp. 890–907, 2008.
- [17] J. Wurz, V. J. Logeeswaran A. Sarkar, and M. S. Islam, "High current density and failure mechanism in epitaxially bridged silicon nanowires," in *8th IEEE Conf. on Nanotechnology*, 2008, pp. 595–597.
- [18] F. P. Incropera, D. P. DeWitt, T. L. Bergman, and A. S. Lavine, *Introduction to Heat and Mass Transfer*, New York, NY, USA: John Wiley & Sons, 2007.

(EPFL), Neuchâtel, Switzerland, in 2010, and at the Max Planck Institute for Solid State Research, Stuttgart, Germany, in 2011.



**Dana Weinstein** is an Associate Professor in electrical engineering and computer science at MIT. She received her B.A. in physics and astrophysics from the University of California–Berkeley in 2004 and her Ph.D. in applied physics in 2009 from Cornell, working on multi-GHz MEMS. Dana is the recipient of the NSF CAREER Award, the DARPA Young Faculty Award, the Intel Early Career Award, and the IEEE IEDM Roger A. Haken Best Paper Award. Her current research focuses on hybrid MEMS-IC devices for low-power

wireless communication, microprocessor clocking, and sensing applications. In particular, she is working to harness the benefits of acoustic vibrations to enhance the performance of next-generation electron devices.



**Subramanian Sundaram** received his B.E. degrees with honors in electrical engineering and mechanical engineering from the Birla Institute of Technology and Science (BITS), Pilani, India, in 2010, the S.M. degree in electrical engineering and computer science from the Massachusetts Institute of Technology (MIT), Cambridge, MA, in 2014, and is currently working towards the Ph.D. degree. He worked on his undergraduate theses at the Ecole Polytechnique Fédérale de Lausanne